Solid–fluid equilibria for hard dumbbells via Monte Carlo simulation

C. Vega,[a] E. P. A. Paras, and P. A. Monson[b]
Department of Chemical Engineering, University of Massachusetts, Amherst, Massachusetts 01003

(Received 24 January 1992; accepted 11 March 1992)

We present the results of a study of solid–fluid phase equilibria in systems of hard dumbbells for three values of the dumbbell bond length. Monte Carlo simulations were used to calculate the equation of state and Helmholtz free energy. Four orientationally ordered solid phases have been considered—the α-N_2 structure and three different base centered monoclinic structures formed by the stacking of hexagonally packed layers that allow the dumbbells to achieve their maximum packing density. In addition, a face-centered-cubic (fcc) plastic crystal was studied for the system with the lowest bond length. The three base centered monoclinic structures have thermodynamic properties which are indistinguishable at the level of accuracy in our calculations. For longer bond lengths, the stable solid structure tends to be orientationally ordered base centered monoclinic. However, we also consider the stability of an aperiodic crystal for the case of dumbbells formed from tangent spheres. At lower bond lengths, the system freezes into a fcc plastic crystal which becomes unstable with respect to a base centered monoclinic structure at higher pressure. The transition between these solid phases is apparently first order. The behavior for the lowest bond length considered resembles that of nitrogen at high temperatures. Our results suggest that the α-N_2 is not a stable crystal structure for hard dumbbell solids at any bond length, but does appear as a metastable phase in some cases.

I. INTRODUCTION

The freezing of hard spheres is considered to provide a good molecular model for the underlying physics in the freezing of the rare gases.[1,2] For relatively simple nonspherical molecules such as N_2, CO_2, or the halogens, a variety of more complicated molecular interactions beyond simple size and shape effects can be expected to play some role in stabilizing the solid in a given crystal structure and hence in determining the solid–fluid equilibria. These might include anisotropic dispersion forces or quadrupole–quadrupole interactions. Nevertheless, it is important to understand how much of the physics of freezing in molecular systems can emerge by only including the size and shape effects. Simple models such as the hard dumbbell and hard ellipsoid are especially important in this context. Such models can be expected to serve as reference systems in perturbation or mean field theories of the solid–fluid equilibria in more complex systems.

Frenkel *et al.*[3-5] have made a comprehensive Monte Carlo simulation study of hard ellipsoids. This study focused principally on the isotropic–nematic transition in the fluid phase for more anisotropic systems, but the solid–fluid equilibria were also obtained. They found that for large anisotropies, the hard ellipsoids freeze into an orientationally ordered solid phase, which may be obtained by performing an affine transformation on the particles in a fcc hard sphere solid. For small anisotropies, they found a fcc plastic crystal to be the stable solid phase on freezing. This transforms into the orientationally ordered phase at higher pressures in a transition which is thought to be second order or weakly first order. Frenkel and co-workers also found that the phase densities and the pressure at freezing exhibited a maximum when plotted vs the molecular anisotropy.

Density functional theory has been extended to hard dumbbells by Smithline *et al.*[6] and by McCoy *et al.*[7] These studies predicted a freezing transition into a fcc plastic crystal for mildly anisotropic systems. However, for anisotropies appropriate to N_2, the plastic crystal phase could not be stabilized relative to the fluid. This result may well be due to the failure of approximations made in the density functional theories. However, until the present work, no simulation results have been present which establish the thermodynamic stability of the plastic crystal phase for hard dumbbell systems with anisotropies appropriate to nitrogen. However, the mechanical stability of the plastic crystal phase at lower anisotropy has been established.[8]

In this paper, we present a fairly extensive study of the solid–fluid equilibria in systems of hard dumbbells for three different elongations. The model we are considering consists of two hard spheres, each of diameter σ, separated by a distance L. We characterize the molecular anisotropy by the reduced bond length or elongation $L^* = L/\sigma$. We have studied systems with $L^* = 0.3$, 0.6, and 1.0. Our principal findings are as follows. For $L^* = 0.6$, the fluid freezes into an orientationally ordered structure. We have examined three orientationally ordered base centered monoclinic structures of this type (formed by stacking hexagonally packed layers of dumbbells) which have identical maximum packing densities and thermodynamic properties which are indistinguishable within the uncertainties of our simulations. These structures are related to those formed by the solid halogens.[9] The α-N_2 structure is mechanically stable, but thermodynamically metastable for the $L^* = 0.6$ solid at moderate pressures, but is unstable for the $L^* = 1.0$ solid. For

---

[a] On leave from: Departamento de Quimica-Fisica, Facultad CC. Quimicas, Universidad Complutense, 28040 Madrid, Spain.

[b] Author to whom correspondence should be addressed.

0021-9606/92/129060-13$06.00

$L^* = 0.3$, the hard dumbbell fluid freezes into a fcc plastic crystal. This phase becomes unstable with respect to the orientationally ordered phase at higher pressure. The α-N_2 structure again appears as a metastable phase at high pressures. For $L^* = 1.0$, we have studied freezing into orientationally ordered close packed structures. For this system, we also have the possibility of forming aperiodic crystals due to the degeneracy of the system.[10–12] Although we have not simulated such structures, we have made an estimate of the extra stability afforded by the degeneracy contribution to the free energy and have used this to estimate the influence on the freezing properties.

The remainder of this paper is organized as follows: In Sec. II, we describe the orientationally ordered structures which allow hard dumbbells to achieve their maximum packing densities. In Sec. III, we describe the Monte Carlo simulation techniques used in this work. We discuss the results in detail in Sec. IV and Sec. V presents our conclusions.

II. STRUCTURES OF HARD DUMBBELLS AT CLOSE PACKING

Although to our knowledge it is not possible to establish *a priori* the stable structure of hard dumbbell solids, it seems to us that in common with hard ellipsoids, the structure at close packing should be a good starting point. To understand the geometry of hard dumbbell solids at closest packing, we begin by noting that hard dumbbells can be arranged into hexagonally packed layers in such a way that each sphere of the dumbbell also lies in a hexagonally packed layer. The dumbbell axis is then tilted from the normal to the hexagonal layer by an angle equal to $\arcsin(L^*/\sqrt{3})$. Each of these layers exposes a hexagonal array of spheres to the layers above and below it. Thus the layers may be stacked like layers of spheres. We have identified three different ways in which the dumbbell layers may be stacked. These are readily illustrated for the case where $L^* = 1.0$ which at closest packing is

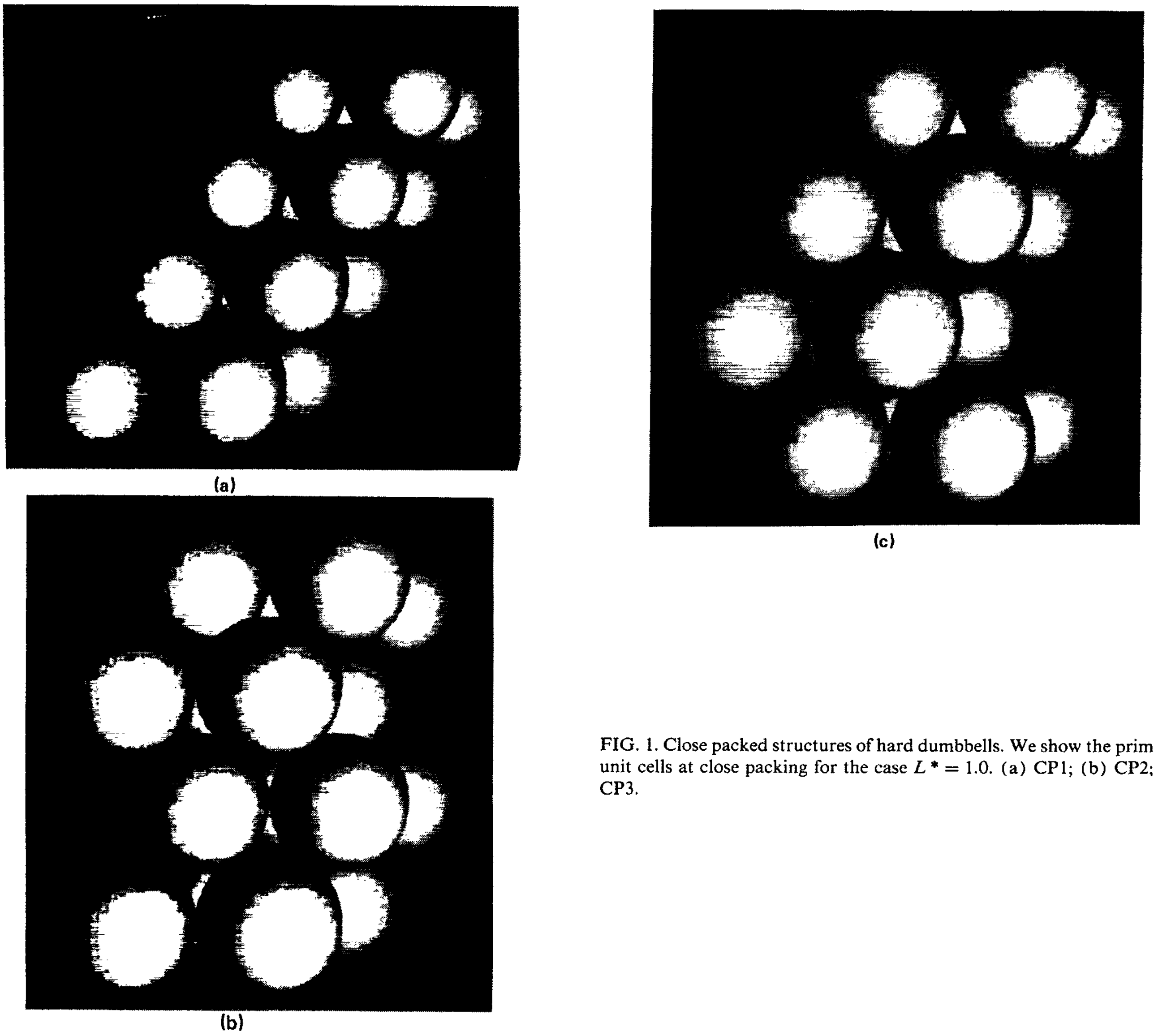

FIG. 1. Close packed structures of hard dumbbells. We show the primitive unit cells at close packing for the case $L^* = 1.0$. (a) CP1; (b) CP2; (c) CP3.

identical in structure to a close packed array of spheres. There are two different ways of stacking the layers in which the dumbbell axes are all parallel. In one of these, the dumbbell spheres are arranged in an ABC sequence so that the structure is a fcc array of spheres. We label this structure CP1. In the other way the dumbbell spheres are stacked in an ABAB sequence so that the structure is a hexagonal close packed (hcp) array of spheres. We label this structure CP2. The layers may also be stacked so that the tilt angle alternates between successive layers. We label this structure CP3. Primitive unit cells for each structure are shown in Fig. 1. Each of these different arrangements has the same maximum packing density, which in reduced units is given by

$$\rho^*_{\rm cp} = \frac{2(1+3/2L^* - L^{*3}/2)}{R\sqrt{3}\cos\zeta}, \tag{2.1}$$

where

$$\sin\zeta = \frac{1}{\sqrt{3}}\,(L^*\cos\xi + \sqrt{3-L^{*2}}\,\sin\xi), \tag{2.2}$$

$$\sin\xi = \frac{\sqrt{9-[L^* + \sqrt{(6-2L^{*2})}\,]^2}}{3R}, \tag{2.3}$$

$$R = [1 + L^{*2} + 2/3L^*(L^* + \sqrt{6-2L^{*2}})\,]^{1/2}. \tag{2.4}$$

The reduced density ρ^* is defined as ρd^3 where d is the diameter of the sphere with the same volume as the dumbbell. Equal values of this reduced density for systems with different L^* correspond to the same volume or packing fraction. Figure 2 shows a plot of $\rho^*_{\rm cp}$ vs L^* together with the result for the α-N_2 structure which is given by

$$\rho^*_{\rm cp}(\alpha\text{-}N_2) = \frac{12\sqrt{3}(1+3/2L^* - 1/2L^{*3})}{(L^* + \sqrt{6-L^{*2}})^3}. \tag{2.5}$$

Notice that the result for the CP structure is always higher than for α-N_2, although they become quite close as L^* becomes small.

The Bravais lattice for the CP1 and CP2 structures is base-centered monoclinic with motif one molecule except when $L^* = 0$, where it is fcc, and when $L^* = 1.0$ for CP2, where it is base-centered orthorhombic. For CP3, the Bravais lattice is base-centered monoclinic with a motif of two molecules except for $L^* = 0$, where it is fcc.

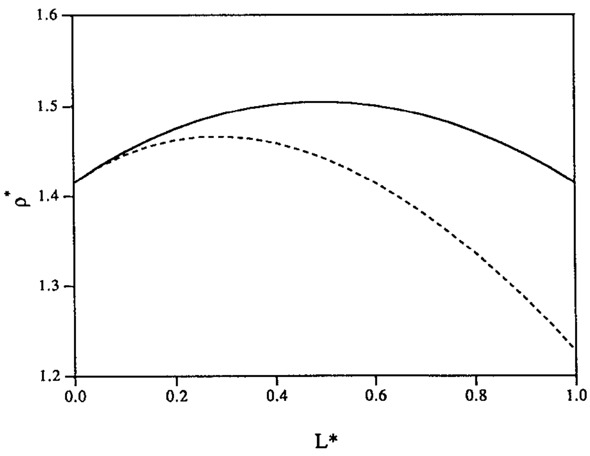

FIG. 2. Maximum packing densities as a function of the molecular elongation L^* for the close packed structures (solid line) and for the α-N_2 structure (dashed line).

For the case of $L^* = 1.0$, it is also possible to pack the dumbbells in orientationally disordered structures in which the spheres of the dumbbell lie on a fcc or hcp lattice, but the centers of mass form an aperiodic structure. Many such structures could be formed by starting with a fcc or hcp array of spheres and randomly assigning bonds between pairs of spheres in such a way as to create an orientationally disordered array of dumbbells. This idea has been explored recently for two-dimensional dumbbells by Wojciechowski *et al.*[10-12] They found that there is a substantial positive contribution to the entropy of such a system which comes from the degeneracy of the aperiodic structure. This negative contribution to the free energy renders the aperiodic structure more stable than the orientationally ordered structures at all densities, even though the effect on the equation of state and the free energy without the contribution from the degeneracy is quite small. We have not simulated such structures in this work, but our results do allow us to make an estimate of the their properties. We will return to this later in the paper.

III. SIMULATION METHODOLOGY

The determination of the solid–fluid equilibria requires the knowledge of the equation of state (EOS) and free energies in both phases. Since we are considering several solid structures as described in the previous section, the EOS and the free energy calculations must be done for each solid structure.

To simulate the solid phase, we used the Monte Carlo (MC) equivalent of the molecular dynamics method developed by Parrinello and Rahman.[13] The method is a constant pressure MC simulation[14] but changes in the unit cell shape are allowed, in contrast to the conventional constant pressure MC.[15] The change in the shape of the unit cell is performed by random displacement in all the elements of the h matrix, h being the matrix which relates the real coordinates $\mathbf{r}(\equiv\{x,y,z\})$ to the scaled coordinates $\mathbf{r}'_i(\equiv\{x',y',z'\})$[13,14] through the expression $\mathbf{r} = h\,\mathbf{r}'_i$. The cell shape changes are important because the equilibrium unit cell shape may change with pressure.

The simulation of the close packed structures involved in most cases a 144 (6×6×4) particle system, but in a few cases, a 486 (9×9×6) particle system was used. For the close packed structures, the initial simulation box shape in the 144 (486) particle system was obtained by stacking six (9) particles in the **a** and **b** directions, four (6) in the **c** direction, and then expanding to the desired density (**a**, **b**, and **c** are the base vectors of the primitive unit cell used in the simulation). In the initial configuration, the **a** axis is coincident with the x Cartesian axis; the **a**–**b** plane lies in the x,y plane. Therefore the initial configuration was not in general cubic. In the case of the α-N_2 lattice, we used 108 particles, although in some cases, 256 particles were used and the initial simulation box was cubic. A run typically involved 20 000 cycles for equilibration and 20 000 for the calculation of thermodynamic averages. A cycle consisted of an attempt to move each particle and an attempt to change the volume and/or shape of the system. A particle move consisted of a combined translation and rotation. The volume change was carried out by a simultaneous random displacement of all the elements of the h matrix, allowing changes in the lengths and orientations of the cell unit basis vectors **a**, **b**, and **c**. The acceptance ratio for the translational–orientational moves was generally about 20%–30%. For the volume change, we found an acceptance ratio of 5%–10% to be the optimum. For some states, we checked that the pressure obtained from the virial theorem was close to the imposed pressure.

To study the orientational ordering, we computed an orientational order parameter defined as[16]

$$S=\frac{1}{N^2}\left\langle \sum_{i=1}^{N} [(2\cos^2\chi_i-1)^2+2\cos\chi_i\sin\chi_i]\right\rangle, \quad (3.1)$$

where χ_i is the angle formed by the particle i with the z Cartesian axis and the brackets denote an ensemble average. This parameter varies between unity if all of the particles have the same value of χ_i and 1/9 if the values of χ_i are uniformly distributed. In addition, we evaluated the normalized probability distribution function for the angles θ and ϕ, θ being the angle formed by the molecular axis with the perpendicular to the **a**–**b** plane and ϕ the angle formed by the projection of the molecular axes on the **a**–**b** plane and the **a** axis. The difference in the definitions of θ and χ allows for the possibility of rotation of the entire simulation cell with respect to space fixed Cartesian coordinates, although this was not observed to any great extent in our calculations. These distribution functions were obtained by using the relations

$$f(\theta)=\left\langle \frac{N(\theta)}{N\sin(\theta)\Delta\theta}\right\rangle, \quad (3.2)$$

$$f(\phi)=\left\langle \frac{N(\phi)}{N\Delta\phi}\right\rangle, \quad (3.3)$$

where $N(\theta)$ and $N(\phi)$ are the number of particles encountered between an angle θ and $\theta+d\theta$ or $\phi+d\phi$. For homonuclear dumbbells, the distribution function $f(\theta)$ has the symmetry property $f(\theta)=f(\pi-\theta)$, while for $f(\phi)$, it holds that $f(\phi)=f(\phi+\pi)$. In the beginning of the simulation, we set θ to less than $\pi/2$. Thus if the symmetry in θ is not assumed, a symmetric $f(\theta)$ will only be obtained when the density is sufficiently low to allow molecular axes to reorient and only after a sufficiently lengthy simulation. In many cases, the length of the run was not enough to get a completely symmetric $f(\theta)$ or $f(\phi)$. This nonsymmetric distribution gives us information about how easy or difficult it is for the molecular axes to reorient at the given density. It should be understood, however, that the true $f(\phi)$ and $f(\theta)$ are indeed symmetric.

To study the translational order, we use the order parameter t_a defined as

$$t_a=\frac{1}{N^2}\left\langle\left[\sum_{i=1}^{N}\cos(2\pi x_i' n_a)\right]^2+\left[\sum_{i=1}^{N}\sin(2\pi x_i' n_a)\right]^2\right\rangle, \quad (3.4)$$

where n_a stands for the number of particles in the **a** direction with identical expressions for t_b and t_c.

Once the EOS for the solid is known, the calculation of the free energy for a state of the solid must be performed so that the chemical potential and phase equilibria can be determined. To that purpose, we used the Frenkel–Ladd[17] method as extended to nonspherical particles by Frenkel and Mulder.[3] We give a brief description of the method and refer the reader to the papers of Frenkel and co-workers[3-5,17] for a more detailed discussion. The basic idea behind the Frenkel–Ladd method is to create a reversible path linking the solid under consideration to a noninteracting Einstein crystal with fixed center of mass for which the partition function is known in a closed form.[17] There are four steps involved. In the first step, the free energy of a noninteracting Einstein crystal with fixed center of mass A_E is determined. The Hamiltonian defining the noninteracting Einstein crystal H_1 is given in the case of a linear molecule by

$$H_1=\lambda_1\sum(\mathbf{r}_i-\mathbf{r}_i^0)^2+\lambda_2\sum\sin^2(\alpha_1)+H_{\text{ideal}}, \quad (3.5)$$

where $\mathbf{r}_i^0$ represents the average position of the center of mass of particle i in the hard dumbbell fluid and α_i is the angle formed by the axes of particle i with the equilibrium position of the axes of particle i in the original hard dumbbell solid. The equilibrium orientations in the hard dumbbell solid are not necessarily the same for all the particles (see, for instance, the α-N_2 or the CP3 lattice). λ_1 and λ_2 are coupling parameters with units of energy/length^2 and energy, respectively, and in this work we shall take their numerical values to be the same. H_{ideal} contains all the contributions to the kinetic energy. After integrating over the momenta, we obtain

$$\frac{A_E}{NkT}=\ln(\Lambda_t^3/l^3)+\ln(\Lambda_r)-\frac{1}{N}\ln(Z_E), \quad (3.6)$$

$$Z_E=\frac{1}{l^{3N}}\int\exp\left\{-\beta\left[\lambda_1\sum(\mathbf{r}_i-\mathbf{r}_i^0)^2+\lambda_2\sum\sin^2(\alpha_i)\right]\right\}d1\cdots dN, \quad (3.7)$$

where $\beta=1/kT$, $d1\equiv d\mathbf{r}_1\,d\omega_1$ (ω denotes a normalized set of orientational coordinates), l is an arbitrary unit of length, $\Lambda_t=(h^2/2\pi mkT)^{1/2}$, and $\Lambda_r=(h^2/8\pi^2IkT)$. Now to determine Z_E, the center of mass of the Einstein crystal is fixed and the partition function (3.7) can be computed analytically. The final expression for A_E is[3]

$$\frac{A_E}{NkT}=\ln(\Lambda_t^3/l^3)+\ln(\Lambda_r)-\ln[J(\lambda_2)]-\frac{1}{N}\ln\left\{N^{-3/2}\left[\frac{\pi}{\lambda_1/(kT/l^2)}\right]^{3/2(N-1)}\right\} \quad (3.8)$$

$$J(\lambda_2)=\int_0^1\exp[\beta\lambda_2(x^2-1)]dx. \quad (3.9)$$

Once the free energy of the noninteracting Einstein crystal with fixed center of mass is known, the next step is to evaluate the difference in free energy ΔA_1 between this and an interacting Einstein crystal for which the Hamiltonian H_2 (excluding the ideal part) is given by

$$H_2 = \lambda_1 \sum (\mathbf{r}_i - \mathbf{r}_i^0)^2 + \lambda_2 \sum \sin^2(\alpha_i) + \sum_{i<j}\sum u_{\rm HD}(i,j). \tag{3.10}$$

Here $u_{\rm HD}(i,j)$ is the pair potential of the hard dumbbell system and is given by

$$u_{\rm HD}(1,2) = \infty \text{ if any } r_{ij} < \sigma, \quad i,j = 1,2 \tag{3.11}$$

and

$$u_{\rm HD}(1,2) = 0 \text{ if all } r_{ij} > \sigma, \quad i,j = 1,2. \tag{3.12}$$

r_{ij} stands for the distance between site i of particle 1 and site j of particle 2. The term ΔA_1 can then be obtained by using umbrella sampling[18] and is then given by

$$\frac{\Delta A_1}{NkT} = -\frac{1}{N}\ln\langle P_E\rangle, \tag{3.13}$$

where $\langle P_E\rangle$ stands for the probability of finding no overlap between hard dumbbells for configurations generated according to the canonical distribution function of the noninteracting Einstein crystal. Since $\langle P_E\rangle$ is less than unity, ΔA_1 is always positive. The values of $\lambda_1^{\max}$ and $\lambda_2^{\max}$ are chosen so that ΔA_1 is small. The next step consists in linking the interacting Einstein crystal with fixed center of mass ($\lambda_1 = \lambda_1^{\max}$, $\lambda_2 = \lambda_2^{\max}$) with the hard dumbbell solid with fixed center of mass ($\lambda_1 = 0, \lambda_2 = 0$). An arbitrary path in the (λ_1, λ_2) plane linking these two points must be chosen. We follow the procedure of Frenkel and Mulder and choose $\lambda_1 = \xi\lambda_1^{\max}$, $\lambda_2 = \xi\lambda_2^{\max}$ where the coupling parameter ξ changes from 1 to 0. If we now define $\lambda_1^* = \lambda_1/(kT/l^2)$, $\lambda_2^* = \lambda_2/(kT)$ and choose $\lambda_1^{\max}$ and $\lambda_2^{\max}$ so that they have the same value in reduced units, then ΔA_2 is given by[3]

$$\frac{\Delta A_2}{NkT} = \int_{\lambda^*_{\max}}^{0} (\Delta^2 + \tau^2)\, d\lambda^*, \tag{3.14}$$

$$\Delta^2 = \frac{1}{Nl^2}\left\langle \sum (\mathbf{r}_i - \mathbf{r}_i^0)^2 \right\rangle_{\lambda_1^* = \lambda_2^* = \lambda^*}, \tag{3.15}$$

$$\tau^2 = \frac{1}{N}\left\langle \sum \sin^2(\alpha_i) \right\rangle_{\lambda_1^* = \lambda_2^* = \lambda^*}. \tag{3.16}$$

Here the brackets stand for canonical average for a system with Hamiltonian given by Eq. (3.10). Since the integrand in Eq. (3.14) is positive, then ΔA_2 is negative.

The last step consists of evaluating the change in free energy ΔA_3 going from the hard dumbbell solid with fixed center of mass to the hard dumbbell solid. ΔA_3 is then given by[17]

$$\Delta A_3/NkT = -\frac{1}{N}\ln(V/l^3). \tag{3.17}$$

The Helmholtz free energy of the hard dumbbell solid at a given density A/NkT is finally obtained from the expression

$$\frac{A}{NkT} = \frac{A_E}{NkT} + \frac{\Delta A_1}{NkT} + \frac{\Delta A_2}{NkT} + \frac{\Delta A_3}{NkT}. \tag{3.17}$$

ΔA_1 and ΔA_2 were obtained by performing constant volume MC runs with 144 (486) particles for the close packed structures and 108 (256) particles for the α-N_2 structure. We used 10 000 cycles for equilibration and 20 000 to obtain thermodynamic averages. To evaluate the integral, we followed the procedure of Ref. 3 and used a ten point Gauss–Legendre quadrature with the transformation described in Ref. 17, which makes the integrand a smooth varying function of the integration variable. The unit cell dimensions used in the free energy calculation at a given density correspond to that obtained by averaging the fluctuating box shape in the constant pressure Monte Carlo simulations. For the close packing structures, we found that the equilibrium shape of the unit cell was very close to that found at close packing, but with a small distortion in the length of the c axes which tend to be generally slightly smaller than at close packing. The same behavior was found by Frenkel and Mulder[3] for the hard ellipsoid solid. For the α-N_2 structure, the system remained cubic at all pressures.

Once the free energy of a given hard dumbbell solid structure has been determined for a given density $A(\rho_1)$, then the free energies at a different density $A(\rho_2)$ can be obtained by thermodynamic integration

$$A(\rho_2)/NkT = A(\rho_1)/NkT + \int_{\rho_1}^{\rho_2} (p/\rho^2 kT)\, d\rho. \tag{3.18}$$

To perform integration in Eq. (3.18), we fitted the pressure to a polynomial. To determine the solid–fluid equilibria, the EOS and Helmholtz free energy of the fluid branch are needed. Tildesley and Streett[19] have performed a number of simulations for the hard dumbbell fluid with different elongations for packing fractions up to 0.4712 and fitted the results to an empirical expression. Since we needed to know the fluid EOS at somewhat higher densities than this, we decided to investigate the accuracy of the Tildesley–Streett equation of state outside the range of states where it was determined. We have performed additional runs at higher pressures with 144 particles (20 000 cycles equilibration and 20 000 cycles for averaging) for hard dumbbells with $L^* = 0.3, 0.6$, and 1.0. The results are shown in Table I along with the predictions of the Tildesley–Streett EOS.[19,20] As can be seen, the Tildesley–Streett EOS agrees very well with the MC results. The predicted densities lie well within 1% of the simulation results which is the estimated uncertainty of the simulation densities. At $L^* = 1.0$, the deviations are slightly larger, but still remain within the uncertainty of the MC results. Since the agreement was found to be good, we used the Tildesley and Streett EOS to describe the fluid behavior of hard dumbbells. By thermodynamic integration of the fluid EOS, the residual part of the free energy can be determined. The solid–fluid equilibria was then determined by equating the pressure and chemical potential in the solid and fluid phases.

To check the computer codes, we have done several tests. We have evaluated the free energy for hard spheres at $\rho^* = 1.0409$ and found good agreement with the results reported by Frenkel and Ladd.[17] We have also checked thermodynamic consistency. For that purpose, we have evaluated the free energy of the CP3 lattice for $L^* = 1.0$ at two different densities ($\rho^* = 1.181$ and $\rho^* = 1.218$) with the Frenkel–Ladd method, and in this way, we found a free energy difference between the states $\Delta A/NkT = 1.01$. By integration of the equation of state, we found that

TABLE I. The equation of state for hard dumbbells with elongations $L^* = 1.0$, 0.6, and 0.3 in the fluid phase as obtained from MC results and from the Tildesley and Streett (TS) (Ref. 19) EOS. Pressures and densities are given in reduced units $p^* = pd^3/kT$ and $\rho^* = \rho d^3$, where d is the diameter of a hard sphere with the same volume as the hard dumbbell.

$L^* = 1.0$ p^*	MC $\langle\rho^*\rangle$	TS $\langle\rho^*\rangle$
15	0.881	0.883
20	0.943	0.942
25	0.979	0.988
30	1.013	1.024
35	1.045	1.055
40	1.072	1.081

$L^* = 0.6$ p^*	MC $\langle\rho^*\rangle$	TS $\langle\rho^*\rangle$
15	0.949	0.955
20	1.021	1.017
25	1.056	1.063
30	1.098	1.100
35	1.125	1.131
40	1.152	1.157

$L^* = 0.3$ p^*	MC $\langle\rho^*\rangle$	TS $\langle\rho^*\rangle$
10	0.900	0.895
15	0.984	0.984
20	1.039	1.045
22.5	1.073	1.070
25	1.092	1.092
27.5	1.116	1.111
30	1.131	1.128
32.5	1.150	1.144

$\Delta A/NkT = 1.02$, which indicates that the two calculations are thermodynamically consistent.

IV. RESULTS AND DISCUSSION

Tables II–VII summarize all our results for the solid EOS and free energies of hard dumbbell systems as well as the results of our phase equilibrium calculations. In Table II, we present the results for the EOS in the solid branch for hard dumbbells with $L^* = 1.0$ for the three close packed structures considered (CP1, CP2, and CP3). For each pressure and structure, we have performed three independent runs with 20 000 cycles equilibration and 20 000 cycles averaging for each and we give the average value of the density from these three runs. The estimated accuracy in the density for a given pressure is about 1%. We started at the highest pressure and then took the last configuration of the previous run as the initial one for the next lower value of the pressure. The EOS of the three close packed structures is almost the same. That situation resembles the case of hard spheres, where the two close packed structures (hcp and fcc) have an almost identical EOS.[21] For some selected states, we show in brackets the value of the orientational order parameter. The particles are highly oriented at all the studied pressures. However, we observed two changes in the unit cell with respect to its structure at close packing. First we observed a decrease of about 3% in the ratio c/a relative to its value at close packing (see Table V). This change in the shape of the unit cell has a significant effect on the computed free energy for a given density as we have observed by repeating the calculation at one state with c/a fixed at the close packed value. For $L^* = 1$ and $\rho^* = 1.181$, the free energy per particle decreases about 0.30 when the ratio $(c/a)/(c/a)_{cp}$ changes from 1 to 0.98. A similar effect was observed by Frenkel and Mulder[3] for hard ellipsoids. The second change accounts for a small shift in the angle θ made by the particles with the direction perpendicular to the layers. For $L^* = 1$, the value of θ at close packing is 35.26°, whereas the observed value of θ during the runs was of about 32°. The computed angle distribution functions $f(\theta)$ and $f(\phi)$ remain sharp with a high peak centered on the equilibrium position.

TABLE II. The equation of state for hard dumbbells with $L^* = 1.0$ in the solid phase. The three close packed structures are considered. Every result represents the average of three independent runs. The number of particles used was 144 except for the results labeled with an asterisk where 486 particles were used. The value of the orientational order parameter is shown between brackets for some selected states.

p^*	CP1 $\langle\rho^*\rangle$	CP2 $\langle\rho^*\rangle$	CP3 $\langle\rho^*\rangle$
20	1.040(0.96)	1.043	1.036
25	1.099	1.106	1.105
30	1.148	1.151	1.139
35	1.174	1.178	1.178
35*	1.174*		
40	1.204(0.99)	1.202	1.200
45	1.224	1.226	1.222
50	1.242	1.244	1.239
50*	1.244*		
55	1.255	1.257	1.254
60	1.264(0.99)	1.265	1.266

TABLE III. The equation of state for hard dumbbells with $L^* = 0.6$ in the solid phase. The three close packed structures and the α-N_2 structures are considered. Every result represents the average of three independent runs. The orientational order parameter is shown between brackets for some selected states.

p^*	CP1 $\langle\rho^*\rangle$	CP2 $\langle\rho^*\rangle$	CP3 $\langle\rho^*\rangle$	α-N_2 $\langle\rho^*\rangle$
30	1.196(0.58)	1.202(0.63)	1.202(0.62)	1.166(0.88)
35	1.231(0.65)	1.237(0.62)	1.236(0.65)	1.196(0.93)
40	1.257	1.254	1.258	1.225
45	1.288(0.98)	1.279(0.96)	1.283(0.92)	1.241(0.95)
50	1.305	1.304	1.303	1.258
55	1.322	1.322	1.320	1.273
60	1.333(0.99)	1.336(0.99)	1.332(0.98)	1.282(0.97)

Another interesting feature concerns the translational order in these systems. For all the pressures, the system was found to be translational ordered. However, at low pressures (in the metastable part of the solid branch), we found the translational order parameter in the **a** and **b** directions to be smaller than the translational order parameter in the **c** direction by about 20% indicating some anisotropy in translational order. (This anisotropy was found to be much smaller for $L^* = 0.6$ or $L^* = 0.3$.) The anisotropy in translational order is reminiscent of that which might be seen in a smectic phase for more elongated particles. In Table V, we show the

TABLE IV. The equation of state for hard dumbbells with $L^* = 0.3$ in the solid phase. The three close packed structures, α-N_2, and the fcc plastic crystal (PC) structures are considered. Every result represents the average of three independent runs. In the column labeled as PC, the states with the asterisk were obtained from expansion of the state $p^* = 45$ of the α-N_2 lattice, while the other three were obtained by compression of the state $p^* = 35$. The orientational order parameter is shown between brackets for some selected states. The states marked "unstable" for the α-N_2 structure are ones where this structure was not mechanically stable and changed into the fcc plastic crystal during the course of the MC run.

p^*	CP1 $\langle\rho^*\rangle$	CP2 $\langle\rho^*\rangle$	CP3 $\langle\rho^*\rangle$	α-N_2 $\langle\rho^*\rangle$	PC $\langle\rho^*\rangle$
20	1.090(0.06)	1.088	1.091(0.05)	Unstable	1.089(0.10)*
25	1.145	1.147	1.147	Unstable	1.125*
30	1.192(0.32)	1.192	1.196(0.47)	Unstable	1.148*
35	1.236(0.56)	1.237	1.241(0.61)	Unstable	1.175(0.10)*
40	1.260	1.264	1.258	Unstable	1.193(0.14)
44					1.212(0.12)
45	1.285(0.73)	1.287	1.282(0.73)	1.271(0.88)	
48					1.230(0.12)
50	1.299	1.297	1.303	1.289	1.234
55	1.312(0.83)	1.315	1.315(0.83)	1.305(0.94)	
60	1.331	1.335	1.325	1.323	

computed free energies of the reference state obtained with the Frenkel–Ladd method and used for the determination of the phase equilibria. In Table VI, the solid–fluid coexistence properties are shown.

The three close packed lattices have almost identical behavior and in particular almost the same densities and pressures at freezing. We cannot within the accuracy of our calculations establish which of these three lattices is the most stable. The problem again resembles that of hard spheres where it is difficult to determine which of the two close packing structures (hcp or fcc) is the most stable at freezing.[17] We did some simulations of the α-N_2 structure for $L^* = 1.0$ using 108 particles. However, we found that the structure was not mechanically stable. Over the course of the run, the simulation cell slowly changed shape from cubic to orthorhombic and the density became indistinguishable from that of the three close packed structures. Figure 3 shows the branches of the equation of state and the fluid–solid equili-

TABLE V. Free energy calculations for hard dumbbells in the CP1, CP2, CP3, α-N_2, or plastic crystal (PC) solid phases. N is the number of particles used, $\lambda_{\max}$ is the maximum value of λ, $\lambda_{\max} = \lambda_1^* = \lambda_2^*$ with $\lambda_1^* = \lambda_1/(kT/\sigma^2)$ and $\lambda_2^* = \lambda_2/kT$, N_λ is the number of points used to integrate Eq. (3.14) using Gauss–Legendre quadrature. R is the ratio c/a divided by its value at close packing [i.e., $R = (c/a)/(c/a)_{cp}$], ρ^* is the reduced density (units are the same as in Table I), ΔA_1, and ΔA_2 are defined in Eqs. (3.13) and (3.14) respectively, and A_{ref} is the absolute Helmholtz free energy at the reference density. All free energies are divided by NkT. The result for hard spheres labeled with an asterisk was taken from Ref. 17.

L^*	Lattice	N	$\lambda_{\max}$	N_λ	R	ρ^*	ΔA_2	ΔA_1	A_{ref}
1.0	CP1	144	8 000	10	0.96	1.180	− 8.727	0.0000	13.34
1.0	CP1	486	8 000	10	0.99	1.174	− 8.836	0.0000	13.28
1.0	CP2	144	8 000	10	0.98	1.181	− 8.721	0.0000	13.35
1.0	CP2	144	8 000	10	1.00	1.181	− 8.453	0.0000	13.62
1.0	CP3	144	8 000	10	0.98	1.181	− 8.728	0.0000	13.34
1.0	CP3	144	8 000	10	0.98	1.218	− 7.716	0.0000	14.35
0.6	α-N_2	108	8 000	10	1.00	1.225	− 10.22	0.0000	11.72
0.6	CP1	144	8 000	10	0.96	1.289	− 9.105	0.0020	12.86
0.6	CP2	144	8 000	10	0.99	1.284	− 9.271	0.0050	12.69
0.6	CP3	144	16 000	10	0.99	1.283	− 10.99	0.0310	12.72
0.3	α-N_2	256	3 000	10	1.00	1.269	− 8.222	0.0081	11.11
0.3	PC	108	1 000	20	1.00	1.090	− 10.16	0.0008	6.39
0.3	PC	108	1 000	20	1.00	1.125	− 9.485	0.0036	7.06
0.3	PC	108	1 000	20	1.00	1.160	− 8.701	0.0122	7.86
0.3	CP1	144	3 000	20	0.94	1.235	− 9.353	0.0156	9.96
0.3	CP2	144	3 000	20	0.97	1.240	− 9.253	0.0272	10.07
0.3	CP3	144	3 000	20	0.94	1.222	− 9.727	0.0448	9.62
0	fcc	125	632.03	5	1.00	1.041	− 2.972	0.0182	4.96
0*	fcc	108	632.03	10	1.00	1.041	− 2.972	0.0177	4.95

TABLE VI. Solid–fluid equilibria of hard dumbbells as obtained from the MC results for the solid EOS (see Tables II–IV) and the free energy calculations shown in Table V. The fluid was described with the Tildesley and Streett (Ref. 19) equation of state. For $L^* = 1.0$, the solid–fluid equilibria for freezing into the CP1 structure was determined by using the free energy calculations for both 144 and 486 particles (see Table V).

$L^* = 1.0$ Lattice	ρ_f^*	ρ_s^*	p^*	μ/kT
CP1 ($N = 144$)	1.053	1.174	34.57	42.64
CP1 ($N = 486$)	1.058	1.179	35.45	43.48
CP2	1.052	1.177	34.37	42.45
CP3	1.051	1.173	34.25	42.34
$L^* = 0.6$ Lattice	ρ_f^*	ρ_s^*	p^*	μ/kT
α-N_2	1.193	1.255	48.59	51.29
CP1	1.146	1.249	37.97	42.22
CP2	1.143	1.244	37.37	41.70
CP3	1.148	1.252	38.33	42.53
$L^* = 0.3$ Lattice	ρ_f^*	ρ_s^*	p^*	μ/kT
PC	1.017	1.070	17.45	22.37
CP1	1.148	1.221	33.22	36.85
CP2	1.148	1.222	33.22	36.85
CP3	1.143	1.218	32.32	36.08

bria for hard dumbbells with $L^* = 1.0$. For the solid, we only plot the results for the CP1 structure since the results for CP2 and CP3 are almost identical.

In view of the similarity of the equation of state and free energies of the three different orientationally ordered structures, we conjecture that the properties of the aperiodic crystal may be similar, apart from the contribution to the free energy arising from the structural degeneracy. Indeed this has been observed by Wojciechewski *et al.*[12] in their study of two-dimensional hard dumbbells with $L^* = 1.0$. This being the case, we can estimate the free energy of an aperiodic structure from that of any of the orientationally ordered structures by adding a contribution from the degeneracy of the aperiodic structure at close packing. Determination of this is the well-known dimer problem on a fcc crystal and, by using series expansion techniques, the contribution to the free energy has been estimated[22] to be $\Delta A_{\mathrm{SD}}/NkT = -\ln 4.5693 = -1.5194$. Assuming that the degeneracy contribution is independent of density, we have used this result together with the free energy and EOS for the CP3 structure to recompute the freezing properties. These estimates are $p^* = 19.4$, $\rho_f^* = 0.936$, and $\rho_s^* = 1.03$. Notice that these are substantially lower than the results for freezing into the orientationally ordered structure. At this point, we should note that the aperiodic structure may also be stable for values of L^* slightly less than 1.0 for densities below close packing, but this will not be the case for $L^* = 0.3$ and 0.6.

TABLE VII. Phase transitions for hard dumbbells with $L^* = 0.3$. The first two lines correspond to transitions between equilibrium phases. The other lines give data for transitions between metastable phases.

Phase 1	Phase 2	ρ_1^*	ρ_2^*	p^*	μ/kT
Fluid	PC	1.017	1.070	17.45	22.37
PC	CP3	1.195	1.262	39.95	42.20
PC	α-N_2	1.233	1.288	49.88	50.37
Fluid	CP3	1.143	1.218	32.32	36.08

In Table III, the EOS for hard dumbbells with $L^* = 0.6$ in the close packed structures and in the α-N_2 structure are shown. The results again correspond to the average of three independent runs. The three close packed structures again have an almost identical EOS. However, the α-N_2 lattice has a significantly different EOS. At a given pressure, the density of the α-N_2 structure is always about 4%–5% less than that of the close packed structures. This is not surprising since the close packing density of α-N_2 for $L^* = 0.6$ is about 6% smaller than the density at close packing of the other structures. This suggests that at high pressures, the α-N_2 structure cannot be the stable one for $L^* = 0.6$. For the close packed lattices, we did not observe any significant change in the shape of the unit cell with respect to the close packed geometry (except that the ratio c/a decreases slightly). However, the orientational order parameter undergoes a drop (some results are given in Table III) between $p^* = 45$ and $p^* = 35$. At $p^* = 40$, the density of the system is such that the mean distance between particles within the same layer is about $1 + L^*/2$, and that is the minimum distance which will allow reorientation on the lattice. In fact, such a reorientation was observed during the simulations at pres-

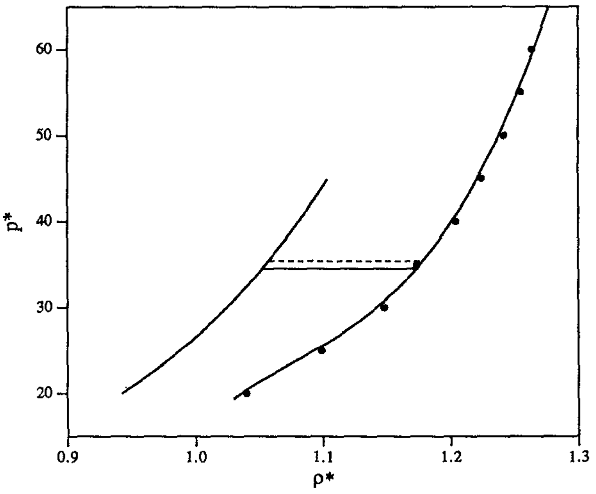

FIG. 3. Solid–fluid equilibria for hard dumbbells with $L^* = 1.0$. The fluid is described with Tildesley and Streett (Ref. 19) EOS. The dots correspond to the MC results for the orientationally ordered solid. The lines through the MC results are a fit of the data. The tie lines connect the states of the orientationally ordered solid and fluid in equilibrium. The solid tie line was obtained by using 144 particles in the free energy calculations, while the dashed tie line was obtained when 486 particles were used in the free energy calculations.

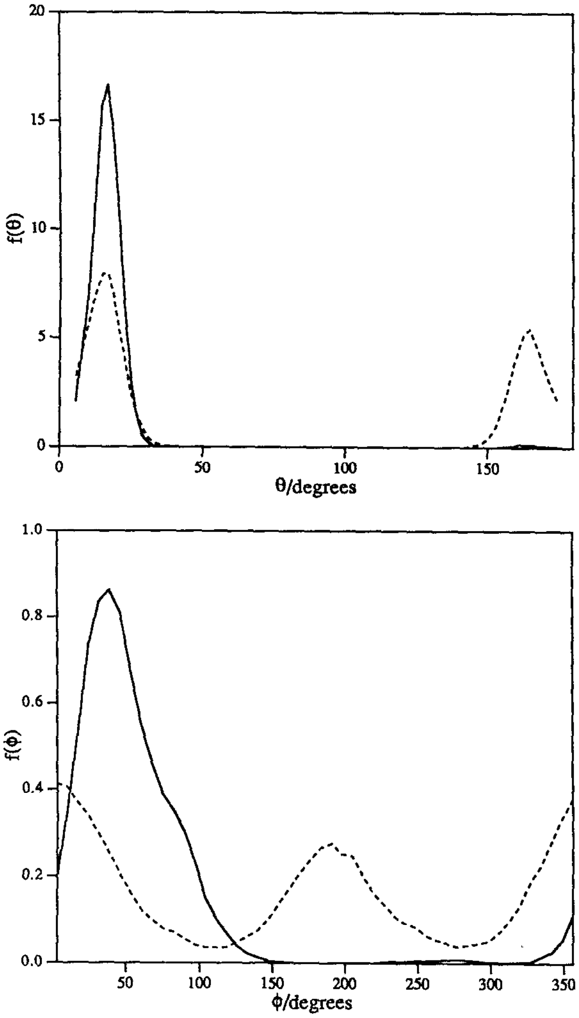

FIG. 4. Angular distributions functions $f(\theta)$ and $f(\phi)$ [see Eqs. (3.2) and (3.3) of the main text] for hard dumbbells with $L^* = 0.6$. The results correspond to the solid structure CP1 at the reduced pressures $p^* = 37.5$ (dashed line) and $p^* = 45$ (solid line).

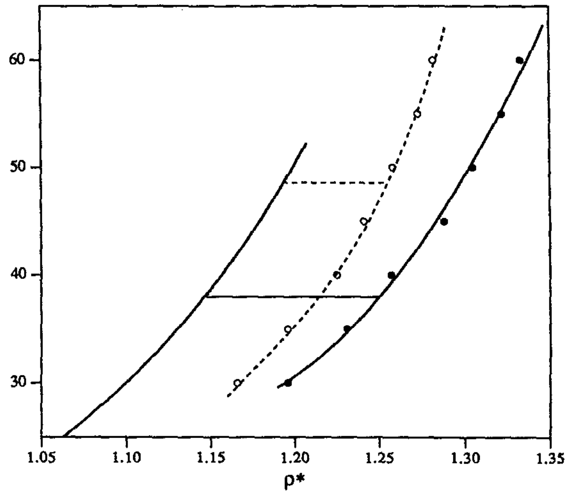

FIG. 5. Solid–fluid equilibria for hard dumbbells with $L^* = 0.6$. The fluid is described with the Tildesley and Streett (Ref. 19) EOS. The filled circles correspond to the MC results for the solid in the CP1 structure and the open circles correspond to the α-N_2 structure. The lines through the MC results are a fit of the data. The tie lines connect the states of the solid and fluid in equilibrium.

sures smaller than $p^* = 40$. Such behavior was not found for $L^* = 1$. In Fig. 4, we show the behavior of $f(\theta)$ and $f(\phi)$ for $p^* = 45$ and $p^* = 37.5$. For $p^* = 45$, $f(\theta)$ are $f(\phi)$ are sharply peaked and no reorientation is observed [note the peak in $f(\theta)$ around 18° and the small value obtained at 180°–18° = 162°]. The peak for $f(\theta)$ is placed around 18° which is slightly smaller than the tilt angle at close packing which is for $L^* = 0.6$ of about 20°. However, for $p^* = 37.5$, a second peak appears in $f(\theta)$ indicating the occurrence of reorientation. Moreover, the distribution $f(\theta)$ is shifted towards smaller angles and significant numbers of particles have their axes perpendicular to the **a–b** plane although most of them remain tilted. The distribution for $f(\phi)$ becomes broader. We conclude that the system, while remaining strongly orientationally ordered, gains significant orientational freedom at about $p^* = 40$.

In Table VI, the results of the solid–fluid equilibria are presented. The solid–fluid transition for α-N_2 occurs at higher pressures than for the close packed structures. Consequently, the hard dumbbell fluid with $L^* = 0.6$ does not freeze into an α-N_2 solid structure. Moreover, by examining the Gibbs free energy vs pressure, we found that for a given pressure the Gibbs energy of the close packed structures is always smaller than that of the α-N_2 structure. Thus for $L^* = 0.6$, the α-N_2 structure is not stable with respect to the close packed structures at any pressure. The densities and pressures at melting of the close packing structures are again very similar and the differences remain within the accuracy of the present calculations. Figure 5 illustrates the branches of the EOS and the fluid–solid equilibria for hard dumbbells with $L^* = 0.6$.

We now turn to the results for $L^* = 0.30$. Table IV shows the results for the EOS for $L^* = 0.3$. The differences between the results for the close packed structures are again very small. As in the case of the longer bond lengths, the ratio c/a decreases as the density is lowered from that at closest packing. The orientational order parameter has values around 0.80 until a pressure of about $p^* = 50$ is reached below which it decreases continuously with decreasing the pressure. Figure 6 shows $f(\theta)$ and $f(\phi)$ for one of the close packed structures at two pressures. The curves are symmetric in all the cases. The molecular axes tend to lie perpendicular to the plane of the layers and the distribution over the angle ϕ is featureless. By decreasing the pressure, the distribution of the angle θ becomes broader.

From Table IV, we can also observe that the density of the α-N_2 lattice for a given pressure is always smaller than that of the close packed structures by about 1%. The maximum packing density of the α-N_2 structure is about 2% less than that of the other structures which helps explain much of the difference. The order parameter always takes high values. However, when the system is simulated at pressures below $p^* = 40$, important changes occur. The results labeled with an asterisk in the column labeled plastic crystal in Table IV were obtained from the expansion of the final configura-

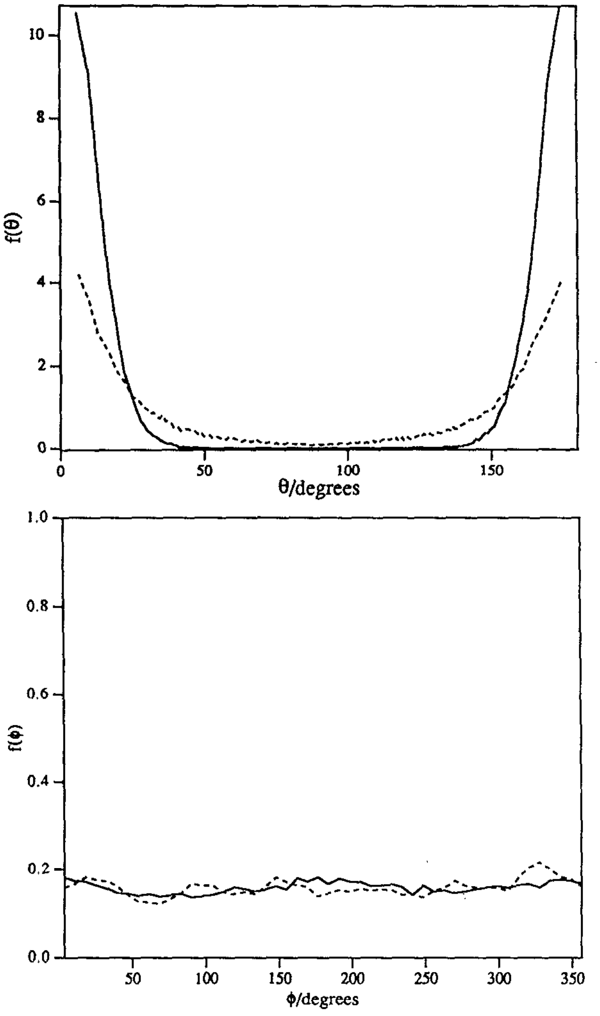

FIG. 6. Angular distributions functions $f(\theta)$ and $f(\phi)$ for hard dumbbells with $L^* = 0.3$. The results correspond to the solid structure CP1 at the reduced pressures $p^* = 30$ (dotted line) and $p^* = 45$ (solid line).

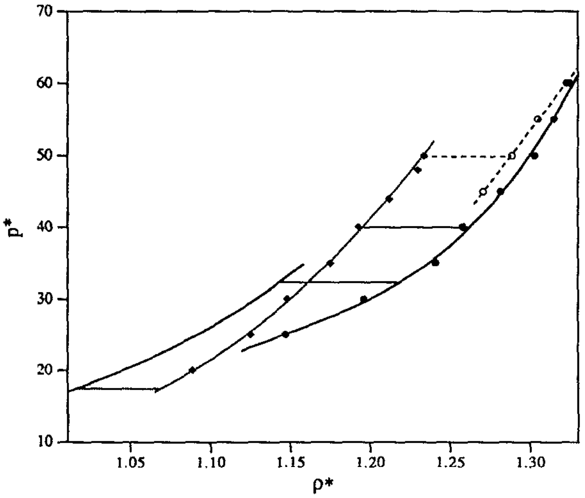

FIG. 7. Solid–fluid equilibria for hard dumbbells with $L^* = 0.3$. The fluid is described with Tildesley and Streett (Ref. 19) EOS. The points correspond to the MC results for the solid (filled circles—CP1; open circles—α-N_2; diamonds—fcc plastic crystal). The lines through the MC results are a fit of the data. The tie lines connect the states (both stable and metastable) in equilibrium.

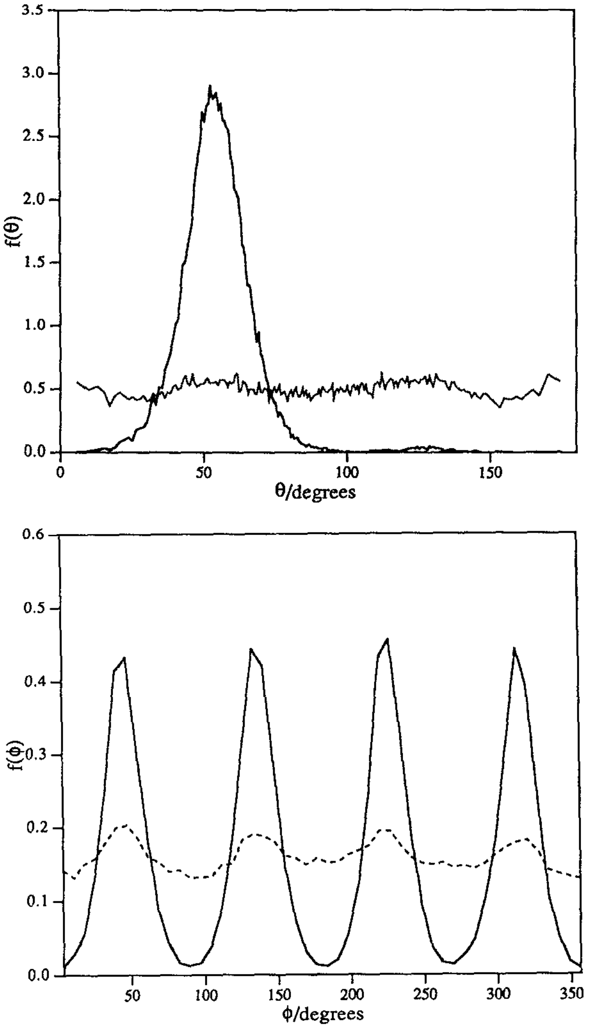

FIG. 8. Angular distribution functions $f(\theta)$ and $f(\phi)$ for hard dumbbells with $L^* = 0.3$. The results are for the structures α-N_2 at $p^* = 45$ (solid line) and fcc plastic crystal at $p^* = 30$ (dotted line).

tion from the simulation of the α-N_2 system at $p^* = 45$. The orientational order parameter has dropped to a value typical of an isotropic distribution. The symmetry of the system is still cubic (as in the α-N_2 structure) and the center-of-mass distribution corresponds to that of a fcc lattice, but with the particles oriented randomly. Moreover, this orientational change is accompanied by an appreciable density change. The system is now a plastic crystal. We also compressed the system starting from the plastic crystal state at $p^* = 35$ and hysteresis was observed. The system remained in a lower density branch with very low value of the orientational order parameter, but with high values of the translational order parameter. Figure 7 shows all the branches of the EOS which we studied for $L^* = 0.3$. In Fig. 8, we show $f(\theta)$ and $f(\phi)$ for the α-N_2 structure at $p^* = 45$ and for the plastic crystal at $p^* = 30$. The distribution of angles is flat for the plastic crystal indicating equal probability for any selected orientation in agreement with the results of Ref. 23. It is interesting to note that Allen and Imbierski[8] found a fcc plastic crystal for hard dumbbells with $L^* = 0.05$, although they did not calculate free energies. For $L^* = 0.3$, they studied one state point of α-N_2 at very high density. Our results show that at lower densities, a first-order phase transition between α-N_2 and the fcc plastic crystal phase would occur. However, we emphasize that even at the high densities, the α-N_2 structure is metastable with respect to the close packed structures.

Our results suggest that the phase transition between α-N_2 and a fcc plastic crystal is first order. To determine the coexistence between these two phases, we have determined the free energy in both of them. The free energy calculations are shown in Table V. We determined the tie line between the coexisting phases to be at $p^* = 50$. This is in agreement with the fact that α-N_2 was found to be mechanically unstable for pressures below $p^* = 40$. The difference in density between the fcc plastic crystal and the α-N_2 structure at the transition is about 4%.

We have determined the solid–fluid transition for the close packed structures and the plastic crystal phase. The results are presented in Table VI. The close packing structures melt at higher pressures than the plastic crystal phase. Note also the difference in the density change for both transitions which is large for the fluid to close packed structure transition and small for the fluid to plastic crystal transition. At low pressures, the fluid is the stable phase and at high pressures the close packing structures are found to be the stable ones. At intermediate range of pressures, the fcc plastic crystal is the stable one. Therefore the sequence of stable equilibrium phases for hard dumbbells with $L^* = 0.3$ (for the structures considered) is fluid to the fcc plastic crystal to close packed structure. The α-N_2 is never stable with respect to the close packed structures. In Table VII, we show all the phases transitions found for $L^* = 0.3$. The first two rows show the transitions between the most stables structures and the next rows are for the transitions occurring between metastable phases which are the fcc plastic crystal to α-N_2 phase transition and the close packed structure to fluid phase transition. Figure 7 shows the tie lines for all the phase transitions found for $L^* = 0.3$.

The phase diagram found for hard dumbbells with $L^* = 0.3$ has some similarities and some differences with the behavior found in N_2.[24] N_2 at liquid temperatures freezes into a hexagonally close packed structure in which there is no long-range orientational order. This phase is called β-N_2 and is a plastic crystal. Upon cooling, β-N_2 undergoes a first-order transition to α-N_2. For hard dumbbells with $L^* = 0.3$ (which corresponds approximately to the anisotropy of N_2), we found the fluid at freezing to be in equilibrium with a plastic crystal, and that this plastic crystal is less stable at higher densities or pressures than the α-N_2 structure (although this is metastable with respect to the close packed structures). Moreover, the density jump at freezing[25] found for N_2 is about 2%, which is small compared with the jump found in other substances. Meijer *et al.*[26] have recently studied the liquid to β-N_2 transition for a realistic model of N_2 at 300 K and found a density change of about 2%. The density change at freezing found in this study for hard dumbbells with $L^* = 0.3$ is about 5% which is about half of that found for $L^* = 0.6$ and $L^* = 1.0$. The relatively small density change on freezing seen for these hard dumbbells and for N_2 is due to the expanded nature of the plastic crystal structure.

Of course β-N_2 and the fcc plastic crystal differ in the arrangement of the center of mass (hcp and fcc, respectively). Although we have not studied the relative stability of the fcc plastic crystal with respect to the β-N_2 structure and therefore we cannot determine which of these two structures is more stable, we believe the free energy differences will be small. Two observations support this argument. The first is that the differences in free energy between hcp and fcc lattices for hard spheres are very small.[17] Second, two theoretical studies[6,7] have found almost no difference in free energy between the hcp and fcc plastic crystals for hard dumbbells of small elongations. Another difference between the hard dumbbell model and N_2 is that in the case of hard dumbbells, the plastic crystal transforms into the close packed structure at higher pressures. However, N_2 transforms from the β-N_2 structure into a number of structures (α,γ,δ) depending on the temperature and pressure. Hard dumbbells should be able to mimic the behavior of N_2 at very high temperatures where the effect of the attractive forces decreases. Under these conditions, it is experimentally observed that liquid N_2 freezes into the β-N_2 structure, then it transforms into δ-N_2 (cubic) and finally into a solid structure which loses its cubic symmetry and seems to be rhombohedral. This resembles the sequence fluid to plastic crystal to close packed structure of the hard dumbbell model. Another important difference is that for hard dumbbells, the α-N_2 structure was never found to be stable, whereas nitrogen exhibits this solid structure at low temperatures. We believe the quadrupole moment of nitrogen to play an important role in stabilizing the α-N_2 structure[9] with respect to the close packed structures at low temperature.

In Fig. 9, we show the dependence on L^* of the solid–fluid coexistence pressures of the hard dumbbell systems

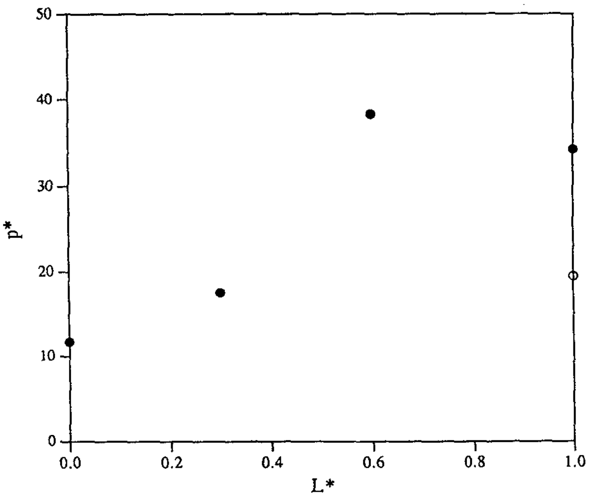

FIG. 9. Coexistence pressures for the solid–fluid equilibria of hard dumbbells as a function of the molecular elongation L^*. The results for hard spheres ($L^* = 0$) are those of Ref. 27. The result indicated by the open circle is our estimate of the coexistence pressure for freezing into an aperiodic crystal for $L^* = 1.0$.

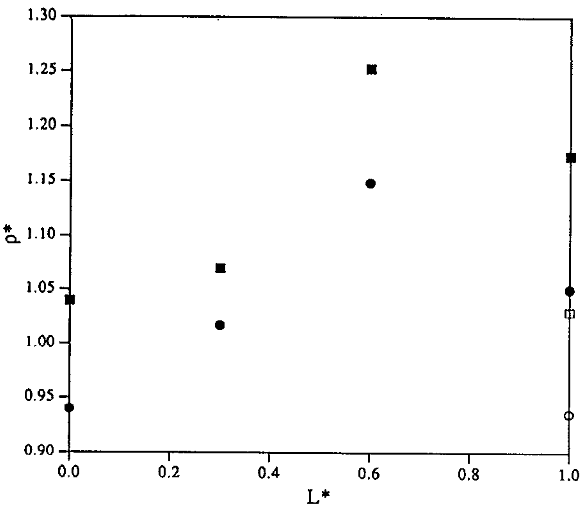

FIG. 10. Densities of the fluid (filled and open circles) and the solid (filled and open squares) at coexistence for hard dumbbells. The results for hard spheres ($L^* = 0$) are those of Ref. 27. The results indicated by the open symbols are our estimates of the coexistence densities for freezing into an aperiodic crystal for $L^* = 1.0$.

found in this work, as well as those of hard spheres.[27] The molecular anisotropy first increases the coexistence pressure with respect to the hard sphere model, it reaches a maximum around $L^* = 0.6$ and then decreases again for higher anisotropies. Figure 10 shows the densities of the fluid and solid at equilibrium for hard dumbbells. The freezing transition for hard dumbbells occurs at higher densities (packing fractions) than for hard spheres. The densities of the fluid and solid at coexistence reach a maximum around $L^* = 0.6$ and then start to decrease. For hard ellipsoids, Frenkel and Mulder[3] also found a maximum in the coexistence pressure and densities as a function of the anisotropy. In both Figs. 9 and 10, we have included our estimate of the freezing properties for $L^* = 1.0$ into the aperiodic structure as well as for the orientationally ordered structures.

The jump in the density at freezing is about 10% for hard dumbbells with $L^* = 0.6$ and $L^* = 1.0$. However, for $L^* = 0.30$, it is only about 5%. The reason for this different behavior is that while hard dumbbells with $L^* = 0.6$ and $L^* = 1.0$ freeze into a close packed structure, hard dumbbells with $L^* = 0.3$ freeze into a fcc plastic crystal. The change in density at freezing for hard spheres ($L^* = 0$) is about 10%. Since we found a density change of 5% for hard dumbbells with $L^* = 0.3$ and since we also expect freezing into the fcc plastic crystal to occur for $L^* < 0.3$, we conjecture that between $L^* = 0$ and $L^* = 0.3$, there is a smooth decrease in the fractional density change.

Finally, we need to address the effect of system size on our results. Frenkel and Ladd[17] have shown for hard spheres that the free energy calculations are especially sensitive to the system size. Although we have not studied systematically the system size dependence of the determined coexistence properties, we have performed some calculations with a system of 486 particles for $L^* = 1.0$ and the CP1 lattice. We performed constant pressure MC simulations at $p^* = 35$ and $p^* = 50$ and the results are shown in Table II. The effect of system size on the EOS is quite small. For the state $p^* = 35$, we have also performed free energy calculations (see Table V) and there is some system size dependence in the determined free energy. In Table VI and in Fig. 3, we compare the coexistence properties obtained with the EOS of the $N = 144$ system together with the free energy obtained from the $N = 486$ system and the differences, although quite small, are not entirely negligible. Nevertheless, they are sufficiently small as to suggest that the main features and trends found in this work do not differ significantly from what might be found with larger system sizes.

V. SUMMARY AND CONCLUSIONS

We have presented a study of the solid–fluid equilibria in systems of hard dumbbells. Five types of solid phase were investigated. We found that for $L^* = 0.6$, the stable solid structure is base centered monoclinic although we were unable to distinguish the relative stability of three structures of this type (CP1, CP2, or CP3). At the shortest bond length considered ($L^* = 0.3$), the fluid freezes into a fcc plastic crystal which becomes unstable with respect to the orientationally ordered close packed structures at higher density. Our results indicate that the α-N_2 structure is not the stable structure for hard dumbbells of any elongation, but appears as a metastable phase. The coexisting pressures and density exhibit a maximum when plotted vs the dumbbell elongation. This is similar to the dependence seen in studies of hard ellipsoids. For $L^* = 0.3$, the results are qualitatively similar to the freezing properties of N_2 at high temperatures in that a plastic crystal is the stable solid phase at freezing and the density change on freezing is small. The stable crystal structures of the hard dumbbells at higher elongations are related to those exhibited by the solid halogens.

For $L^* = 1.0$, we have studied freezing into orientationally ordered close packed structures. For this system, we also have the possibility of forming an aperiodic crystal. Although we have not simulated such a structure, we have made an estimate of the extra stability afforded by the structural degeneracy contribution to the free energy and have used this to estimate the influence on the freezing properties. We estimate that the aperiodic structure would be substantially more stable than the orientationally ordered structures, and the freezing pressure and densities are also significantly lower. Some simulations of the equation of state and free energy of the aperiodic structure will be necessary to test the accuracy of these estimates.

We hope that the simulation data presented here will be useful in testing different theoretical approaches to the determination of solid–fluid equilibria of hard nonspherical models such as the density functional theories.[6,7] In this context, we have found that the simple Lennard-Jones and Devonshire[28] cell theory provides quite accurate predictions of equation of state and free energy of the orientationally ordered solid phases considered in this work and when used together with the Tildesley–Streett EOS for the fluid phase predicts correctly the trends in the coexistence properties with the hard dumbbell elongation.[29]

ACKNOWLEDGMENTS

This work was supported by a grant from the U.S. Department of Energy, Office of Basic Energy Sciences. One of us (C.V.) would like to thank the North American–Spanish Fulbright committee for the award of a postdoctoral grant. We are also grateful to the referee for some helpful comments on the paper.

[1] A. D. J. Haymet, Science **236**, 1076 (1987).

[2] H. C. Longuet-Higgins and B. Widom, Mol. Phys. **8**, 549 (1964).

[3] D. Frenkel and B. M. Mulder, Mol. Phys. **55**, 1171 (1985).

[4] D. Frenkel, B. M. Mulder, and J. P. McTague, Phys. Rev. Lett. **52**, 287 (1984).

[5] D. Frenkel, B. M. Mulder, and J. P. McTague, Mol. Cryst. Liq. Cryst. **123**, 119 (1985).

[6] S. J. Smithline, S. W. Rick, and A. D. J. Haymet, J. Chem. Phys. **88**, 2004 (1988).

[7] J. D. McCoy, S. Singer, and D. Chandler, J. Chem. Phys. **87**, 4853 (1987).

[8] M. P. Allen and A. A. Imbierski, Mol. Phys. **60**, 453 (1987).

[9] C. A. English and J. A. Venables, Proc. R. Soc. London, Ser. A **340**, 57 (1974).

[10] A. C. Branka and K. W. Wojciechowski, Mol. Phys. **56**, 1149 (1985).

[11] K. W. Wojciechowski, Phys. Lett. A **122**, 377 (1987).

[12] K. W. Wojciechowski, D. Frenkel, and A. C. Branka, Phys. Rev. Lett. **66**, 3168 (1991).

[13] M. Parrinello and A. Rahman, Phys. Rev. Lett. **45**, 1196 (1980).

[14] R. Najafabadi, S. Yip, Scr. Metallogr. **17**, 1199 (1983); S. Yashonath and C. N. R. Rao, Mol. Phys. **54**, 245 (1985).

[15] W. W. Wood, J. Chem. Phys. **48**, 415 (1968).

[16] B. C. Freasier, D. Jolly, and R. J. Bearman, Mol. Phys. **31**, 255 (1976).

[17] D. Frenkel and A. J. C. Ladd, J. Chem. Phys. **81**, 3188 (1984).

[18] J. P. Valleau and G. M. Torrie, in *Statistical Mechanics A, Modern Theoretical Chemistry*, edited by B. J. Berne (Plenum, New York, 1977), Vol. 5, p. 178.

[19] D. J. Tildesley and W. B. Streett, Mol. Phys. **41**, 85 (1980).

[20] T. Boublik and I. Nezbeda, Coll. Czech. Chem. Commun, **51**, 2301 (1986).

[21] G. Jackson and F. van Swol, Mol. Phys. **65**, 161 (1988).

[22] J. F. Nagle, Phys. Rev. **152**, 190 (1966).

[23] J. Belak, R. LeSar, and R. D. Etters, J. Chem. Phys. **92**, 5430 (1990).

[24] T. A. Scott, Phys. Rep. C **27**, 89 (1976).

[25] R. L. Mills, D. H. Liebenberg, and J. C. Bronson, J. Chem. Phys. **63**, 4026 (1975).

[26] E. J. Meijer, D. Frenkel, R. A. LeSar, and A. J. C. Ladd, J. Chem. Phys. **92**, 7570 (1990).

[27] W. G. Hoover and F. H. Ree, J. Chem. Phys. **49**, 3609 (1968).

[28] J. E. Lennard-Jones and A. F. Devonshire, Proc. R. Soc. London, Ser. A **163**, 53 (1937).

[29] E. P. A. Paras, C. Vega, and P. A. Monson, Mol. Phys. (in press).